Realization of broadband ultrasonic chiral Landau levels in an elastic metamaterial

Yafeng Chen [1], Zhihao Lan [2], Lei Fan [3], Shanjun Liang [4], Liang An [3,*], Jie Zhu [1,†] and Zhongqing Su [3,‡]

[1] *Institute of Acoustics, School of Physics Science and Engineering, Tongji University, Shanghai 200092, China*

[2] *Department of Electronic and Electrical Engineering, University College London, London WC1E 7JE, United Kingdom*

[3] *Department of Mechanical Engineering, The Hong Kong Polytechnic University, Kowloon, Hong Kong SAR, China*

[4] *School of Professional Education and Executive Development, The Hong Kong Polytechnic University, Hong Kong SAR, China*

(Received 28 November 2024; revised 7 April 2025; accepted 9 April 2025; published 5 May 2025)

Metamaterials with Landau levels induced by synthetic pseudomagnetic fields present an exciting avenue for manipulating elastic waves. Traditionally, these Landau levels in elastic metamaterials are generated by out-of-plane pseudomagnetic fields, resulting in flat-band dispersions with limited bandwidth. In this study, we develop an elastic metamaterial with broadband ultrasonic chiral Landau levels induced by in-plane pseudomagnetic fields, which are synthesized by introducing linearly increased effective Dirac mass via locally breaking the inversion symmetry of each unit cell. We experimentally observe broadband zeroth-order chiral Landau levels for ultrasonic energy transmission. Additionally, we report the experimental observation of snake states, arising from the interaction between zeroth-order and first-order Landau levels. The excellent robustness of the chiral Landau levels is also experimentally validated. Our work suggests a way for realizing broadband ultrasonic chiral Landau levels in elastic systems, with promising potential for applications in engineering devices for integrated communication of elastic waves.

DOI: 10.1103/PhysRevB.111.184303

I. INTRODUCTION

Many interesting phenomena in condensed matter physics, such as Landau quantization and quantum Hall physics, are related to the behaviors of electrons under external magnetic fields. Unlike electrons, which are charged fermions, photons or phonons, as the quanta of classical electromagnetic waves or mechanical vibrations, are neutral bosons and as a result, they do not couple directly to real magnetic fields. It has been known that inhomogeneous strains applied to a graphene sheet can induce pseudomagnetic fields coupled to Dirac fermions in the effective low-energy description of graphene [1–3]. As this strain-induced pseudomagnetic field is a geometrical effect, it can be conveniently transferred to classical wave systems. Indeed, strain-induced pseudomagnetic fields and Landau levels have been studied in both photonic [4–13] and acoustic [14,15] systems in the past. Essentially, the effect of strain leads to a shift of the Dirac points in the two-dimensional (2D) momentum space, which could be interpreted as an effective vector gauge potential. While the strain in general deforms the whole lattice, which may be challenging to implement in practice, modifying the unit cell itself in a regular 2D lattice could also shift the Dirac points in momentum space and pseudomagnetic fields generated in this way have also been explored [16–20].

The gauge potential $\mathbf{A} = (A_x, A_y)$ generated by shifting the Dirac points in the (k_x, k_y) momentum space is in plane, which means the pseudomagnetic field ($B_z = \nabla \times \mathbf{A}$) is perpendicular to the x-y plane. The Landau levels induced by such out-of-plane pseudomagnetic field in general are dispersiveless flat bands. While these flat Landau bands have high density of states, which can be useful for enhancing light-matter interactions, the waves associated with these flat bands are localized and can not propagate through the system. Apart from Dirac point degeneracy, flat Landau bands can also arise from ring degeneracy [21–24]. Importantly, it has also been known that dispersive chiral Landau levels can emerge at 3D Weyl points under external magnetic fields [25–28]. The chiral Landau level is a topologically protected one-way bulk state with its propagation direction determined by the direction of the external magnetic field and the net number of such levels determined by the topological charge of the corresponding degenerate point [29]. Up to now, chiral Landau levels have been studied in three dimensions [30–32] and two dimensions [33–37]. Towards on-chip applications, Cui *et al.* realize chiral Landau levels in an integrated elastic platform with pillars [36]. It is still desirable to develop a compact platform with perforated holes towards different application scenarios, such as developing topological phononic thin film.

In this work, we theoretically propose an ultrasonic elastic metamaterial platform for chiral Landau levels and experimentally investigate their propagation characteristics. The chiral Landau levels are induced by an in-plane pseudomagnetic field, which is realized by linearly modulating the position-dependent effective mass of the Dirac phonons via locally breaking the inversion symmetry of the unit cell. The propagation and dispersion properties of the zeroth-order chiral Landau levels are clearly observed in experiments on ultrasonic energy transmission. Moreover, by exciting both

*Contact author: liang.an@polyu.edu.hk

†Contact author: jiezhu@tongji.edu.cn

‡Contact author: zhongqing.su@polyu.edu.hk

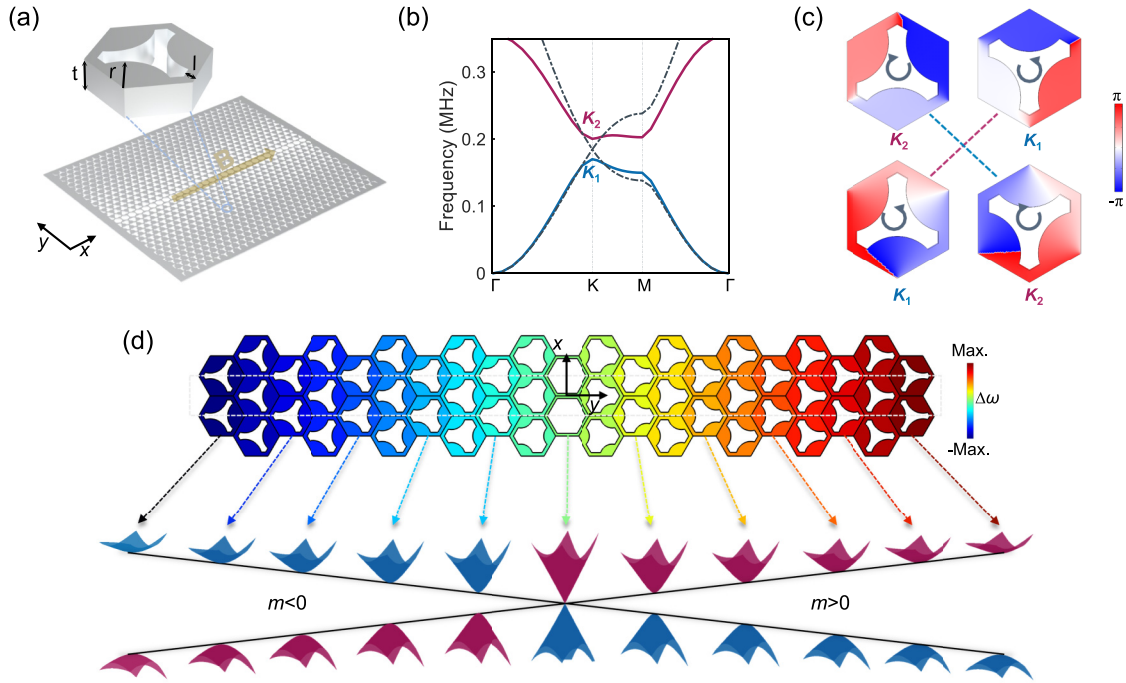

FIG. 1. Design of the system with synthetic in-plane pseudomagnetic fields. (a) Schematic of the system and the unit cell. (b) Band diagrams of the unit cell ($r = l = 0.069a$) with the Dirac cone (dashed lines) and the unit cell ($r = 0.414a$, $l = 0.1a$) with a band gap (solid lines). (c) Phase distributions of the eigenmodes around the K valley of the first and second bands for the unit cell ($r = 0.414a$, $l = 0.1a$) and its inversion-symmetric partner. (d) Illustration of the principle to synthesize an in-plane pseudomagnetic field by linearly opening the local band gap $\Delta\omega$ at the Dirac point of each unit cell along the y axis. The bottom panel shows the representative dispersion surfaces around the K valley of the unit cells in the top panel.

the zeroth- and first-order Landau levels, snake states are also observed. Finally, excellent robustness of the chiral Landau levels against a step path and defects benefiting from the large-area nature of these states is also experimentally validated. These findings provide a paradigm for the manipulation of ultrasonic elastic waves via pseudomagnetic field-induced chiral Landau levels and may offer promising opportunities for the design of compact elastic wave devices.

II. EMERGENCE OF CHIRAL LANDAU LEVELS INDUCED BY IN-PLANE PSEUDOMAGNETIC FIELDS

We begin by describing the system and the principle for synthesizing the in-plane pseudomagnetic fields. The elastic system we considered is a microperforated phononic plate as shown in Fig. 1(a). The material of the plate is aluminum with the elastic modulus, density, and Poisson ratio of 70 GPa, 2700 kg/m^3, and 0.33, respectively. The unit cell [see the inset of Fig. 1(a)] is made of three one-third disks with radius of r, which are connected by the slender rods with width of l. The lattice size and thickness of the unit cell are $a = 3$ mm and $t = 0.93$ mm. We mainly consider the out-of-plane flexural modes of the system in this work, which support Dirac cones at the K/K' points of the Brillouin zone when the unit cell has the inversion symmetry [see Fig. 1(b)]. The Hamiltonian describing the Dirac phonons around the K/K' valleys could be written as $H_D = v_D(\eta k_x\sigma_x + k_y\sigma_y)$ ($\hbar = 1$), where v_D denotes the Dirac velocity; $\eta = \pm 1$ corresponds to the K and K' valleys; k_x and k_y are the relative wave vectors with respect to the K/K' valleys; σ_x and σ_y are the Pauli matrices. Moreover, one can open a band gap at the Dirac point by breaking the inversion symmetry of the unit cell [see Fig. 1(b)], which essentially introduces an effective mass term $m\sigma_z$ into the Dirac Hamiltonian H_D, i.e., $H_D^m = v_D(\eta k_x\sigma_x + k_y\sigma_y) + m\sigma_z$ with the size of the band gap $\Delta\omega = 2m$. Note that the phases of the eigenmodes at the valley point of the first and second bands corresponding to a unit cell and its inversion-symmetric partner are inverted [see Fig. 1(c)], which means their band gap and effective Dirac mass are also opposite to each other.

According to the substitution rule for a particle with charge of q in electromagnetic fields with vector potential of $\mathbf{A}$, i.e., $\mathbf{k} \to \mathbf{k} + q\mathbf{A}$, one can interpret the effective mass term $m\sigma_z$ in H_D^m as an out-of-plane vector potential of $A_z = m$. Furthermore, if we can make A_z position dependent, then an in-plane pseudomagnetic field via $\mathbf{B} = \nabla \times \mathbf{A}$ can be induced. To realize the in-plane pseudomagnetic fields, in this work we consider a scenario where the local band gap of each unit cell along the y axis has a linear dependence on y, i.e., $m = \gamma y$, which corresponds to a constant pseudomagnetic field of $B_x = \partial_y A_z = \gamma$ [see the schematic yellow arrow in Fig. 1(a)]. In particular, by varying r and l, we construct 11 unit cells, where the local band gap $\Delta\omega$ is linearly increased from zero to a maximum value of $\Delta\omega_{\max}$ with a step of $\Delta\omega_{\max}/10$ along the $+y$ direction, and arrange their inversion-symmetric partners along the $-y$ direction (see Sec. 1 of the Supplemental Material [38] for the detailed geometrical parameters of these unit cells), as shown in Fig. 1(d). Under such a configuration, the system is no longer periodic along the y axis, which means we should replace $k_y \to -i\partial_y$ in H_D^m whereas k_x can still be treated as a good quantum number.

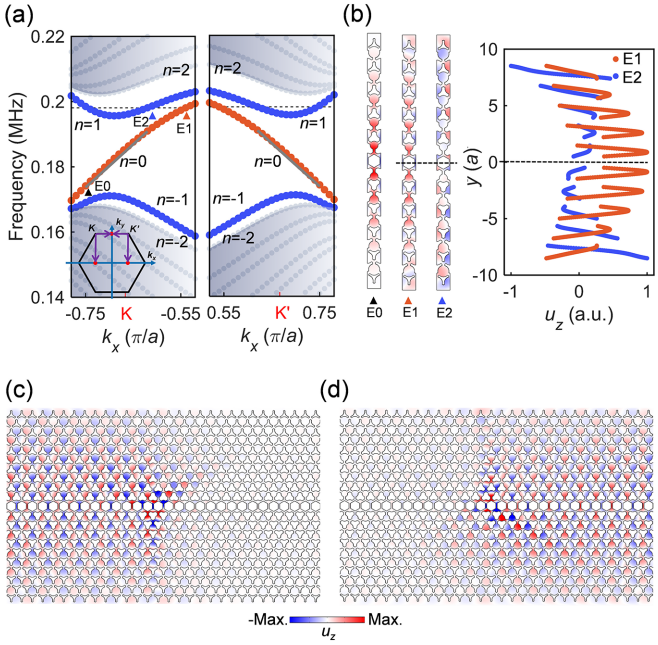

FIG. 2. Emergence of chiral Landau levels. (a) Projected band diagrams of the supercell denoted by the dashed box in Fig. 1(d) around the K and K' valleys, where the first few Landau levels are highlighted. (b) Representative eigenmode of the zeroth-order Landau level [E0, denoted by the black triangle in (a)] at 1.75 MHz, and the symmetric [E1, denoted by the red triangle in (a)] and antisymmetric [E2, denoted by the blue triangle in (a)] eigenmodes of the zeroth-order and first-order Landau levels at 1.98 MHz; the right panel shows the real parts of the eigenmodes E1 and E2 along the y axis. (c) Leftward and (d) rightward one-way propagation of the zeroth-order Landau levels excited by a chiral source.

The quantized Landau levels corresponding to the eigenvalues of $H_D^m = v_D(\eta k_x \sigma_x - i\partial_y \sigma_y) + \gamma y \sigma_z$ could be written as [25,30,33] (see also Sec. 2 of the Supplemental Material [38] for detailed derivation),

$$\omega_n = \begin{cases} \mathrm{sgn}(\gamma)\eta v_D k_x, & n = 0 \\ \pm\sqrt{v_D^2 k_x^2 + 2n|\gamma| v_D}, & n \geqslant 1. \end{cases} \tag{1}$$

Figure 2(a) shows the projected band diagrams of the supercell [denoted by the dashed box in Fig. 1(d)] around the K and K' valleys under periodic boundary conditions along the x direction. It is observed that quantized Landau levels emerge, with the zeroth-order Landau level exhibiting a broad bandwidth, which aligns well with the theoretical solution indicated by the solid line. The eigenmode of the zeroth-order Landau level (indicated by the black triangle) shown in Fig. 2(b) demonstrates that its energy distributes within the central region across a wide length of the supercell, facilitating the large-area transmission of elastic waves. In Sec. 3 of the Supplemental Material [38], we further demonstrate that the field confinement of the zeroth-order eigenmodes can be controlled by adjusting the strength of the pseudomagnetic field, which does not affect the group velocity of the zeroth-order Landau level as shown by Eq. (1). Because the zeroth-order Landau levels locked to the K and K' valleys have opposite group velocities [as per Fig. 2(a)], we can use a chiral source

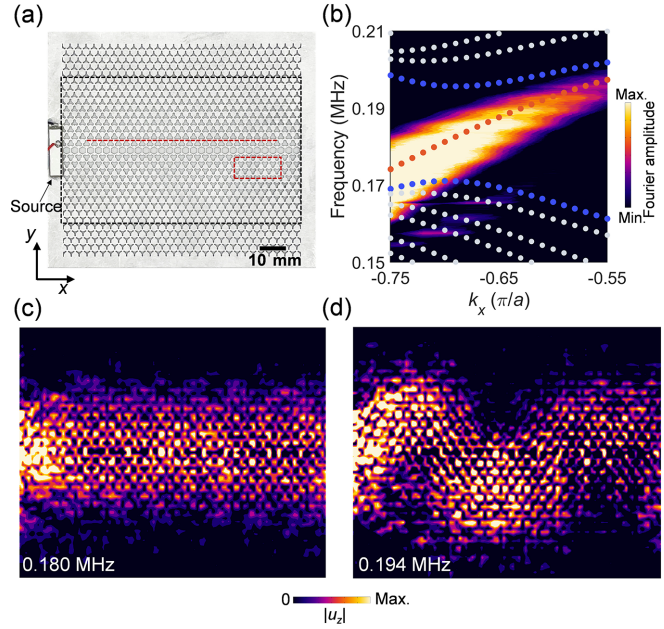

FIG. 3. Experimental validation of the Landau levels. (a) Photograph of the fabricated sample. (b) Experimentally measured projected band diagram, which is obtained by performing the Fourier transform on scanned out-of-plane displacement fields along the red dashed line in (a). Experimentally measured displacement fields of the whole sample at (c) 0.180 MHz and (d) 0.194 MHz, respectively.

for u_z in the middle of the supercell to excite the leftward and rightward one-way propagating waves selectively, as demonstrated in Figs. 2(c) and 2(d). We would like to note that the K and K' valleys project to k_x and k_y directions differently. When the in-plane pseudomagnetic field is along y, they project to the same location along k_y and thus the two chiral Landau levels intersect in the projected band diagram [33], for which the projection process is shown in the insert of Fig. 2(a). In our case, the in-plane pseudomagnetic field is along x and thus the K and K' valleys project to different locations along k_x and consequently, the two chiral Landau levels do not intersect in the projected band diagram [see Fig. 2(a)].

III. EXPERIMENTAL VALIDATION OF THE LANDAU LEVELS AND THEIR ROBUSTNESS

To experimentally validate the Landau levels, we fabricate the sample as shown in Fig. 3(a). The structure within the dashed box of Fig. 3(a) is made by the supercell [indicated by the dashed box in Fig. 1(d)] periodically arranged along the x direction. To mitigate the boundary effect, it is further cladded with several layers of the unit cells with $\Delta\omega_{\max}$, which does not change the dispersions of the Landau levels (see Sec. 4 of the Supplemental Material [38]). A piezoelectric patch is put at the left end of the sample to excite the rightward propagating elastic waves. The excitation force is exerted to be perpendicular to the x-y plane to avoid exciting the in-plane modes. The experimental details are given in Sec. 5 of the Supplemental Material [38]. We first scan the out-of-plane displacements u_z along the red dashed line in Fig. 3(a), based on which the Fourier transform gives the

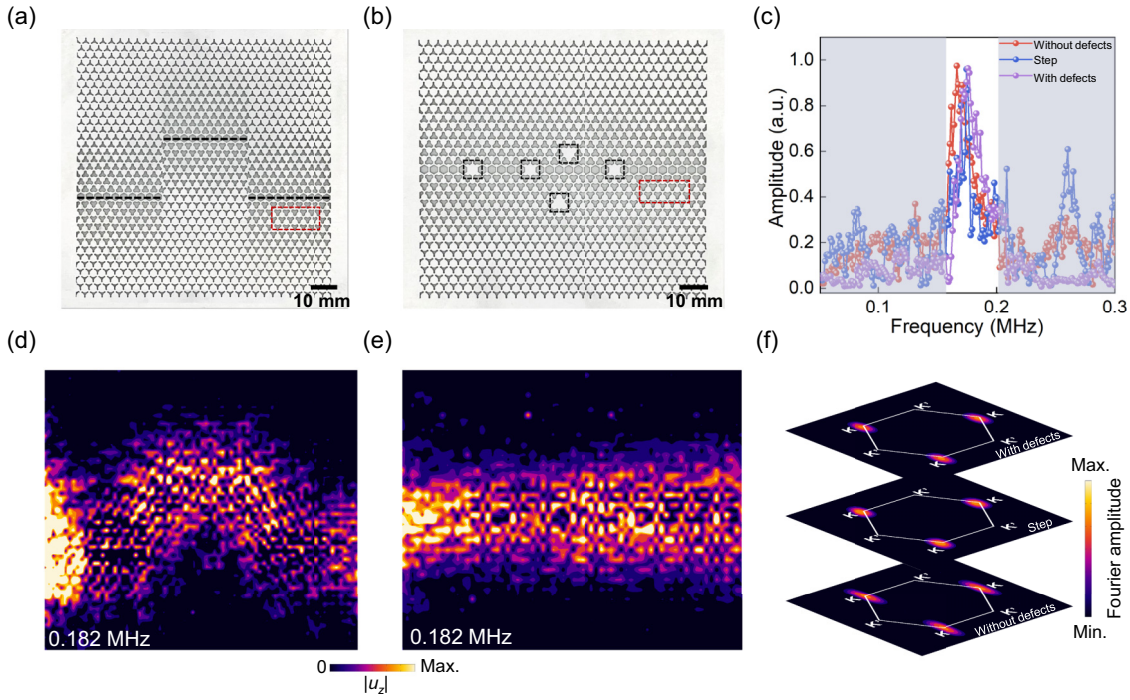

FIG. 4. Demonstration of the robustness of the chiral Landau levels. Photograph of the sample with (a) a step path and (b) defects. (c) Experimentally measured transmission spectra of the three samples, i.e., without defects, with a step path and with defects. Experimentally measured displacement fields of (d) the sample with step path and (e) defects. (f) Fourier spectra obtained by the displacement fields within the red dashed boxes of the three samples in (a), (b) and Fig. 3(a).

dispersions of the eigenmodes along k_x [see Fig. 3(b)]. We can see that the experimentally measured zeroth-order agrees well with the numerical solutions denoted by the red and blue points, respectively. The scanned out-of-plane displacement fields of the whole sample at 0.180 MHz, as plotted in Fig. 3(c), demonstrate the large-area elastic energy conveying via the zeroth-order Landau level. We also present the measured fields at other frequencies in Sec. 6 of the Supplemental Material [38], showing the broadband large-area energy transportation capacities of the zeroth-order Landau level. Notably, we also observe the snakelike propagation at 0.194 MHz, as shown in Fig. 3(d). Such snake state [40–44] is an interesting transport phenomenon arising from the interaction between the zeroth-order and first-order Landau levels with symmetric and antisymmetric eigenmodes about $y = 0$ [as per E1 and E2 in Fig. 2(b)]. The theoretical explanation about the formation of the snake state can be found in Sec. 7 of the Supplemental Material [38].

One can expect that the chiral Landau levels would exhibit strong robustness compared to conventional topological edge states due to their large-area nature. To demonstrate this, we fabricate two samples. The first sample, shown in Fig. 4(a), features a step along the propagation path (indicated by the black dashed line) achieved by shifting the middle domain upward by $4\sqrt{3}a$. The second sample, illustrated in Fig. 4(b), includes several defects created by filling in the holes, as marked by the black dashed boxes. From the measured transmission spectra shown in Fig. 4(c) of the three samples, i.e., the defect-free sample in Fig. 3(a), the sample with a step path in Fig. 4(a), and the sample with defects in Fig. 4(b), we observe distinct transmission peaks within the frequency range between Landau levels with order from $n = -2$ to $n = 2$. From the scanned displacement fields at 0.182 MHz as shown in Figs. 4(d) and 4(e), it is evident that elastic waves can navigate through the step path and bypass the defects. Furthermore, the Fourier transform of the displacement fields within the red dashed boxes in Figs. 3(a), 4(a), and 4(b), as shown in Fig. 4(f), reveals that the propagating elastic waves consistently remain locked at the K valley, unaffected by the step and defects. These experimental results confirm the excellent robustness of elastic wave propagation mediated by the chiral Landau levels.

IV. CONCLUSION AND OUTLOOK

In conclusion, we have achieved broadband ultrasonic chiral Landau levels in an elastic metamaterial, which are induced by in-plane pseudomagnetic fields synthesized through a linear variation of the local band gap around the Dirac point. The dispersion diagram of the chiral Landau levels is experimentally measured, which agrees well with the theoretical calculation. We demonstrate the large-area transmission of ultrasonic energy at approximately 0.18 MHz. Additionally, we observe the snakelike propagation of ultrasonic elastic waves, resulting from the interaction between the zeroth-order and first-order Landau levels. The robustness of the chiral Landau levels has also been experimentally validated. This proposed structure offers a pathway for creating ultrasonic elastic wave devices capable of robust, broadband, and large-area ultrasonic energy transmission. Furthermore, the structure, which hosts zeroth-order Landau levels and snake states with distinct propagation paths and frequencies, provides a foundation for

engineering on-chip elastic demultiplexers. With advanced nanolithography technology, it is anticipated that this structure can be further miniaturized to enable robust, large-area energy transport of GHz elastic waves.

ACKNOWLEDGMENTS

This work is supported by the University-Industry Collaborative Education Program of Ministry of Education of PRC (220804972162224), the National Natural Science Foundation of China (Grants No. 92263208 and No. 12102134), the National Key R&D Program of China (Grants No. 2022YFA1404400 and No. 2022YFA1404403), the Fundamental Research Funds for the Central Universities, the Research Grants Council of Hong Kong SAR (Grants No. 15214323, No. 15200922, No. 15202820, and No. AoE/P-502/20), [Hong Kong Innovation and Technology Commission via project "Smart Railway Technology and Applications" Grant No. K-BBY1], and Faculty Development Scheme (FDS) RGC Project (No. UGC/FDS24/E04/21).

DATA AVAILABILITY

The data that support the findings of this article are not publicly available. The data are available from the authors upon reasonable request.

[1] F. Guinea, M. I. Katsnelson, and A. K. Geim, Energy gaps and a zero-field quantum Hall effect in graphene by strain engineering, Nat. Phys. **6**, 30 (2010).

[2] N. Levy, S. A. Burke, K. L. Meaker, M. Panlasigui, A. Zettl, F. Guinea, A. H. C. Neto, and M. F. Crommie, Strain-induced pseudo–magnetic fields greater than 300 tesla in graphene nanobubbles, Science **329**, 544 (2010).

[3] C. Si, Z. Suna, and F. Liu, Strain engineering of graphene: A review, Nanoscale **8**, 3207 (2016).

[4] M. C. Rechtsman, J. M. Zeuner, A. Tunnermann, S. Nolte, M. Segev, and A. Szameit, Strain-induced pseudomagnetic field and photonic Landau levels in dielectric structures, Nat. Photon. **7**, 153 (2013).

[5] H. Schomerus and N. Y. Halpern, Parity anomaly and Landau-level lasing in strained photonic honeycomb lattices, Phys. Rev. Lett. **110**, 013903 (2013).

[6] O. Jamadi, E. Rozas, G. Salerno, M. Milicevic, T. Ozawa, I. Sagnes, A. Lemaitre, L. L. Gratiet, A. Harouri, I. Carusotto, J. Bloch, and A. Amo, Direct observation of photonic Landau levels and helical edge states in strained honeycomb lattices, Light Sci. Appl. **9**, 144 (2020).

[7] M. Bellec, C. Poli, U. Kuhl, F. Mortessagne, and H. Schomerus, Observation of supersymmetric pseudo-Landau levels in strained microwave graphene, Light Sci. Appl. **9**, 146 (2020).

[8] C.-R. Mann, S. A. R. Horsley, and E. Mariani, Tunable pseudomagnetic fields for polaritons in strained metasurfaces, Nat. Photon. **14**, 669 (2020).

[9] J. Guglielmon, M. C. Rechtsman, and M. I. Weinstein, Landau levels in strained two-dimensional photonic crystals, Phys. Rev. A **103**, 013505 (2021).

[10] Z.-T. Huang, K.-B. Hong, R.-K. Lee, L. Pilozzi, C. Conti, J.-S. Wu, and T.-C. Lu, Pattern-tunable synthetic gauge fields in topological photonic graphene, Nanophoton. **11**, 1297 (2022).

[11] Z. Qi, H. Sun, G. Hu, C. Deng, W. Zhu, B. Liu, Y. Li, S. Liu, X. Yu, and Y. Cui, Electrical manipulation of lightwaves in the uniaxially strained photonic honeycomb lattices under a pseudomagnetic field, Photon. Res. **11**, 1294 (2023).

[12] R. Barczyk, L. Kuipers, and E. Verhagen, Observation of Landau levels and chiral edge states in photonic crystals through pseudomagnetic fields induced by synthetic strain, Nat. Photon. **18**, 574 (2024).

[13] M. Barsukova, F. Grise, Z. Zhang, S. Vaidya, J. Guglielmon, M. I. Weinstein, L. He, B. Zhen, R. McEntaffer, and M. C. Rechtsman, Direct observation of Landau levels in silicon photonic crystals, Nat. Photon. **18**, 580 (2024).

[14] Z. Yang, F. Gao, Y. Yang, and B. Zhang, Strain-induced gauge field and Landau levels in acoustic structures, Phys. Rev. Lett. **118**, 194301 (2017).

[15] H. Abbaszadeh, A. Souslov, J. Paulose, H. Schomerus, and V. Vitelli, Sonic Landau levels and synthetic gauge fields in mechanical metamaterials, Phys. Rev. Lett. **119**, 195502 (2017).

[16] C. Brendela, V. Peanoa, O. J. Painterd, and F. Marquardt, Pseudomagnetic fields for sound at the nanoscale, Proc. Natl. Acad. Sci. USA **114**, E3390 (2017).

[17] X. Wen, C. Qiu, Y. Qi, L. Ye, M. Ke, F. Zhang, and Z. Liu, Acoustic Landau quantization and quantum-Hall-like edge states, Nat. Phys. **15**, 352 (2019).

[18] M. Yan, W. Deng, X. Huang, Y. Wu, Y. Yang, J. Lu, F. Li, and Z. Liu, Pseudomagnetic fields enabled manipulation of on-chip elastic waves, Phys. Rev. Lett. **127**, 136401 (2021).

[19] P. Li, W. Chen, J. Chen, W. Luo, and D. Zhao, Acoustic Landau levels in a synthetic magnetic field with a symmetric gauge, Phys. Rev. Appl. **22**, 014047 (2024).

[20] B. Yang, X. Shen, L. Shi, Y. Yang, and Z. H. Hang, Nonuniform pseudo-magnetic fields in photonic crystals, Adv. Photon. Nexus. **3**, 026011 (2024).

[21] J.-W. Rhim and Y. B. Kim, Landau level quantization and almost flat modes in three-dimensional semimetals with nodal ring spectra, Phys. Rev. B **92**, 045126 (2015).

[22] M.-C. Jin, Z.-G. Chen, M.-H. Lu, P. Zhan, and Y.-F. Chen, Flat Landau levels and interface states in two-dimensional photonic crystals with a nodal ring, Phys. Rev. B **109**, 054108 (2024).

[23] Z. Fu, R. Zheng, J. Liang, J. Lu, W. Deng, M. Ke, X. Huang, and Z. Liu, Pseudomagnetic fields in bilayer phononic crystals, Europhys. Lett. **146**, 46004 (2024).

[24] Z. Cheng, Y.-J. Guan, H. Xue, Y. Long, S.-Q. Yuan, H.-X. Sun, B. Zhang, Three-dimensional flat Landau levels in an inhomogeneous acoustic crystal, Nat. Commun. **15**, 2174 (2024).

[25] H. B. Nielsen and M. Ninomiya, The Adler-Bell-Jackiw anomaly and Weyl fermions in a crystal, Phys. Lett. B **130**, 389 (1983).

[26] D. I. Pikulin, A. Chen, and M. Franz, Chiral anomaly from strain-induced gauge fields in Dirac and Weyl semimetals, Phys. Rev. X **6**, 041021 (2016).

[27] A. G. Grushin, J. W. F. Venderbos, A. Vishwanath, and R. Ilan, Inhomogeneous Weyl and Dirac semimetals: Transport in axial magnetic fields and Fermi arc surface states from pseudo-Landau levels, Phys. Rev. X **6**, 041046 (2016)

[28] R. Ilan, A. G. Grushin, and D. I. Pikulin, Pseudo-electromagnetic fields in 3D topological semimetals, Nat. Rev. Phys. **2**, 29 (2020).

[29] W. Wu, Z.-M. Yu, X. Zhou, Y. X. Zhao, and S. A. Yang, Higher-order Dirac fermions in three dimensions, Phys. Rev. B **101**, 205134 (2020).

[30] X. Yuan, Z. Yan, C. Song, M. Zhang, Z. Li, C. Zhang, Y. Liu, W. Wang, M. Zhao, Z. Lin, T. Xie, J. Ludwig, Y. Jiang, X. Zhang, C. Shang, Z. Ye, J. Wang, F. Chen, Z. Xia, D. Smirnov *et al.*, Chiral Landau levels in Weyl semimetal NbAs with multiple topological carriers, Nat. Commun. **9**, 1854 (2018).

[31] H. Jia, R. Zhang, W. Gao, Q. Guo, B. Yang, J. Hu, Y. Bi, Y. Xiang, C. Liu, and S. Zhang, Observation of chiral zero mode in inhomogeneous three-dimensional Weyl metamaterials, Science **363**, 148 (2019).

[32] V. Peri, M. S. Garcia, R. Ilan, and S. D. Huber, Axial-field-induced chiral channels in an acoustic Weyl system, Nat. Phys. **15**, 357 (2019).

[33] H. Jia, M. Wang, S. Ma, R.-Y. Zhang, J. Hu, D. Wang, and C. T. Chan, Experimental realization of chiral Landau levels in two-dimensional Dirac cone systems with inhomogeneous effective mass, Light Sci. Appl. **12**, 165 (2023).

[34] Y. Yang, J. Zhang, B. Yang, S. Liu, W. Zhang, X. Shen, L. Shi and Z. H. Hang, Photonic Dirac waveguide in inhomogeneous spoof surface plasmonic metasurfaces, Nanophoton. **13**, 3847 (2024).

[35] S. Li, P. G. Kevrekidis, and J. Yang, Emergence of elastic chiral Landau levels and snake states, Phys. Rev. B **109**, 184109 (2024).

[36] Z. Cui, C. Wu, Q. Wei, M. Yan, and G. Chen, On-chip elastic wave manipulations based on synthetic dimension, Phys. Rev. Lett. **133**, 256602 (2024).

[37] Y. Liu, K. Li, W. Liu, Z. Zhang, Y. Cheng, and X. Liu, Observation of chiral Landau levels in two-dimensional acoustic system, Quantum Front. **3**, 26 (2024).

[38] See Supplemental Material at http://link.aps.org/supplemental/10.1103/PhysRevB.111.184303 for the detailed geometrical parameters of unit cells (UCs) for constructing in-plane synthetic pseudomagnetic fields, the theoretical derivation of Landau levels, the effects of the strength of the synthetic pseudomagnetic field on the zeroth-order Landau level, the effects of cladding layers on the dispersions of Landau levels, the experimental details, visualization of the broadband large-area transportation of elastic waves, the emergence of snake states, and effects of the in-plane modes, which also contains Ref. [39].

[39] Y. Chen, L. Fan, J. Zhu, and Z. Su, An all-polarized elastic topological metamaterial for ultrasonic energy conveying and harvesting, Adv. Funct. Mater. **35**, 2413285 (2025).

[40] L. Oroszlany, P. Rakyta, A. Kormanyos, C. J. Lambert, and J. Cserti, Theory of snake states in graphene, Phys. Rev. B **77**, 081403(R) (2008).

[41] J. R. Williams and C. M. Marcus, Snake states along graphene $p-n$ junctions, Phys. Rev. Lett. **107**, 046602 (2011).

[42] T. Taychatanapat, J. Y. Tan, Y. Yeo, K. Watanabe, T. Taniguchi, and B. Ozyilmazm, Conductance oscillations induced by ballistic snake states in a graphene heterojunction, Nat. Commun. **6**, 6093 (2015).

[43] P. Rickhaus, P. Makk, M.-H. Liu, E. Tovari, M. Weiss, R. Maurand, K. Richter, and C. Schonenberger, Snake trajectories in ultraclean graphene $p-n$ junctions, Nat. Commun. **6**, 6470 (2015).

[44] O. M. Bahrova, S. V. Koniakhin, A. V. Nalitov, and E. D. Cherotchenko, Optical snake states in a photonic graphene, Opt. Lett. **49**, 2581 (2024).